



Published in final edited form as:

Exp Neurol. 2016 January ; 275(0 1): 46–58. doi:10.1016/j.expneurol.2015.09.008.

An *Scn1a* epilepsy mutation in *Scn8a* alters seizure susceptibility and behavior

Christopher D. Makinson¹, Karoni Dutt², Frank Lin³, Ligia A. Papale¹, Anupama Shankar¹, Arthur J. Barela², Robert Liu⁴, Alan L. Goldin^{2,*}, and Andrew Escayg^{1,*}

¹Department of Human Genetics, Emory University, Atlanta, GA, 30022

²Department of Microbiology and Molecular Genetics, University of California Irvine, Irvine, CA, 92697

³The Wallace H. Coulter Department of Biomedical Engineering, Georgia Institute of Technology and Emory University, Atlanta, GA 30332

⁴Department of Biology, Emory University, Atlanta, GA, 30022

Abstract

Understanding the role of *SCN8A* in epilepsy and behavior is critical in light of recently identified human *SCN8A* epilepsy mutations. We have previously demonstrated that *Scn8a^{med}* and *Scn8a^{med-jo}* mice carrying mutations in the *Scn8a* gene display increased resistance to flurothyl and kainic acid-induced seizures; however, they also exhibit spontaneous absence seizures. To further investigate the relationship between altered *SCN8A* function and epilepsy, we introduced the *SCN1A*-R1648H mutation, identified in a family with generalized epilepsy with febrile seizures plus (GEFS+), into the corresponding position (R1627H) of the mouse *Scn8a* gene. Heterozygous R1627H mice exhibited increased resistance to some forms of pharmacologically and electrically induced seizures and the mutant *Scn8a* allele ameliorated the phenotype of *Scn1a*-R1648H mutants. Hippocampal slices from heterozygous R1627H mice displayed decreased bursting behavior compared to wild-type littermates. Paradoxically, at the homozygous level, R1627H mice did not display increased seizure resistance and were susceptible to audiogenic seizures. We furthermore observed increased hippocampal pyramidal cell excitability in heterozygous and homozygous *Scn8a*-R1627H mutants, and decreased interneuron excitability in heterozygous *Scn8a*-R1627H mutants. These results expand the phenotypes associated with disruption of the *Scn8a* gene and demonstrate that an *Scn8a* mutation can both confer seizure protection and increase seizure susceptibility.

*To whom correspondence should be addressed: Andrew Escayg, Department of Human Genetics, Emory University, 615 Michael Street, Whitehead Building, Suite 301, Atlanta, GA, 30322, USA, Tel.: (404) 712-8328; Fax: (404) 727-3949; aescayg@emory.edu, or Alan Goldin, Department of Microbiology and Molecular Genetics and Anatomy and Neurobiology, University of California, Irvine, CA 92697-4025, USA, Tel.: (949) 824-5334; Fax: (949)-824-8504, agoldin@uci.edu.

The content is solely the responsibility of the authors and does not necessarily represent the official views of the NIH.

Publisher's Disclaimer: This is a PDF file of an unedited manuscript that has been accepted for publication. As a service to our customers we are providing this early version of the manuscript. The manuscript will undergo copyediting, typesetting, and review of the resulting proof before it is published in its final citable form. Please note that during the production process errors may be discovered which could affect the content, and all legal disclaimers that apply to the journal pertain.

Keywords

Na_v1.6; Na_v1.1; Audiogenic seizure; voltage sensor; sodium channel; GEFS+; Dravet Syndrome; interneuron

INTRODUCTION

Voltage-gated sodium channels (VGSCs) are important regulators of neuronal excitability and are responsible for the initiation and propagation of action potentials in neurons. Given their fundamental role in neuronal communication, disruptions in VGSC function can lead to a host of pathophysiological conditions. Most notably, mutations in the four VGSCs that are primarily expressed in the CNS—*SCN1A* (Na_v1.1), *SCN2A* (Na_v1.2), *SCN3A* (Na_v1.3), and *SCN8A* (Na_v1.6)—are responsible for several types of idiopathic epilepsy. Specifically, *SCN1A* mutations lead to genetic epilepsy with febrile seizures plus (GEFS+) and Dravet syndrome (DS) (Claes et al., 2001; Escayg et al., 2000), *SCN2A* mutations cause benign familial neonatal-infantile seizures (Heron et al., 2002), mutations in *SCN3A* have been identified in patients with partial epilepsy (Estacion et al., 2010; Holland et al., 2008; Vanoye et al., 2014), and *SCN8A* mutations are responsible for some cases of epileptic encephalopathies (EIEE13) (Carvill et al., 2013; Vaher et al., 2013; Veeramah et al., 2012).

Based on the VGSC mutations that have been identified to date, it is clear that distinct seizure and behavioral outcomes can result from different mutations in the same VGSC gene, with the magnitude and direction of the observed phenotypes potentially reflecting specific biophysical changes caused by the mutation. For example, within the spectrum of *SCN1A* epilepsies, the most severe condition, DS, often results from null mutations in the *SCN1A* gene, while amino acid substitutions that change the biophysical properties of the channel can give rise to less severe forms of epilepsy such as GEFS+ (Claes et al., 2009; Escayg and Goldin, 2010; Lossin, 2009).

SCN8A mutations were recently identified in several patients with epileptic encephalopathies (de Kovel et al., 2014; Estacion et al., 2014; O'Brien and Meisler, 2013; Vaher et al., 2013; Veeramah et al., 2012). Functional analyses initially suggested that increased channel activity was the likely biophysical consequence of these mutations (Estacion et al., 2014; Veeramah et al., 2012). However, the recent identification of potential loss-of-function *SCN8A* mutations in this disorder indicates that epilepsy might result from a range of alterations in *SCN8A* activity (de Kovel et al., 2014). The relationship between *SCN8A* dysfunction and disease outcome is also complex as illustrated by the cognitive and motor deficits, but not epilepsy, that were previously observed in a family with a *SCN8A* loss-of-function truncation mutation (Trudeau et al., 2006).

The introduction of clinically relevant VGSC mutations into mouse models has proven critical to our understanding of the functional consequences of distinct VGSC mutations on seizure and behavioral phenotypes. Mice expressing human *SCN1A* mutations recapitulate many of the clinical features of DS and GEFS+ (Martin et al., 2010; Yu et al., 2006), and have led to the “loss of inhibition” model of DS (Yu et al., 2006). Similarly, mice with loss-of-function *Scn8a* mutations exhibit behavioral alterations that are consistent with some

psychiatric findings in patients (McKinney et al., 2008; Papale et al., 2010). Interestingly, we demonstrated that mutations that reduce the activity of *Scn8a* in the mouse confer resistance to induced seizures (Hawkins et al., 2011; Martin et al., 2007), but result in the generation of absence epilepsy (Papale et al., 2009). Recently, the *SCN8A* N1768D gain-of-function mutation, identified in a patient with epileptic encephalopathy, was introduced into the mouse *Scn8a* gene. Mice expressing this mutation exhibited spontaneous seizures, reduced lifespan, impaired motor coordination and deficits in social interaction (Wagnon et al., 2014).

To gain insight into the spectrum of seizure and behavioral outcomes that can arise when the same mutation is expressed in different VGSC genes, we generated a mouse mutant in which the well-characterized *SCN1A* mutation R1648H, first identified in a family with GEFS+ (Escayg et al., 2000), was knocked into the corresponding location in the mouse *Scn8a* gene. The mutant line (*Scn8a*-R1627H) was evaluated for seizure susceptibility, spontaneous seizure generation, behavioral deficits, and neuronal excitability.

MATERIAL AND METHODS

Generation of Construct and Electrophysiology in *Xenopus oocytes*

For expanded methods refer to Supplemental Materials and Methods. We introduced the *Scn1a*-R1648H mutation plus two additional silent substitutions into exon 26 of the *Scn8a* cDNA plasmid for expression in *Xenopus laevis oocytes*. Sodium currents were recorded by two-electrode voltage-clamp.

Generation of mice expressing the *Scn8a* R1627H mutation

A targeting construct consisting of a 4.5-kb 5' arm of homology, the R1627H substitution, a neomycin cassette flanked by *FLP1* recombinase (Fft) sites, and a 4-kb 3' arm of homology, was electroporated into 129X1/SvJ-derived PAT-5 embryonic stem (ES) cells at the University of Michigan Transgenic Core. PCR analysis and Southern blotting were performed to identify correctly targeted ES cells.

Animal breeding and maintenance

All experimental procedures were performed in accordance with the guidelines of Emory University and the University of California, Irvine Institutional Animal Care and Use Committees. All mice were housed in a temperature and humidity controlled vivarium and provided drinking water and food *ad libitum*. R1627H targeted mice were crossed to mice carrying FLP recombinase to remove the neomycin cassette included in the targeting vector. Male mutants were then crossed to female C57BL6/J wild-type (WT) mice for three generations. Heterozygous males and females from this generation (N3) were crossed to generate WT, heterozygous (*Scn8a*^{RH/+}), and homozygous (*Scn8a*^{RH/RH}) mice (N3F1) for experiments. A cohort of N3F1 mice were monitored, weighed, and videotaped weekly from P10 to P120 in order to assess locomotor function and to make general assessments of health and survival. Male *Scn8a*^{RH/+} mice (N3 generation) were also crossed to female C3/HeJ mice for three generations to generate progeny for EEG analysis.

To generate mice carrying both the *Scn8a*-R1627H and the *Scn1a*-R1648H mutations, *Scn8a*^{RH/+} (N3) females were first crossed to *Scn1a*^{RH/+} (N10) males to produce *Scn8a*^{RH/+}/*Scn1a*^{RH/+} offspring. *Scn8a*^{RH/+}/*Scn1a*^{RH/+} males were then crossed to N10 *Scn1a*^{RH/+} females to produce WT, *Scn8a*^{RH/+}, *Scn1a*^{RH/+}, *Scn8a*^{RH/+}/*Scn1a*^{RH/+}, *Scn1a*^{RH/RH}, and *Scn8a*^{RH/+}/*Scn1a*^{RH/RH} offspring.

Genotyping of mutants

Genotyping of R1627H mutant mice was performed by PCR analysis of DNA extracted from tail biopsies. A PCR product spanning the R1627H position was amplified using the following primers: (RH F, AAG ACA GGT TAT CTG TGT AAA CTG; RH R, AAT CGG TTT TGT CTG CAA GAC TGG) to produce a 600bp (R1627H) or a 500bp (WT) product. Genotyping of *Scn1a* R1648H mutant mice was performed as previously reported (Martin et al., 2010).

Protein extraction and Western blot analysis

Protein extraction and Western blot analysis was performed as previously described (Makinson et al., 2014). Detailed methods can be found in Supplemental Materials and Methods.

Animal behavior

All behavioral procedures were conducted between the hours of 10:00 AM and 3:00 PM to minimize possible circadian rhythm effects.

Locomotor activity was measured by photobeam breaks of individually housed mice (San Diego Instruments, La Jolla, CA, USA) over a 24-hour period. Ambulations were counted as consecutive beam breaks.

Rotarod performance was assessed by measuring the latency to fall from an accelerating rotating rod (Columbus Instruments, Rotamex-5 1.3). Each mouse was trained to walk on the rod three times per day for three days. Training trials were 5 minute duration at 5 r.p.m., with each training trial separated by 60 minutes. Mice that fell from the rod during the training trial were placed back on the rod. Following training, rod acceleration was increased in 0.2 r.p.m. increments every second starting at 0 r.p.m. and reaching a maximum of 50 r.p.m. Falls were detected by photobeam break.

Stride length was determined by measuring the distance between paw prints as mice walked across a 5 cm wide 60 cm long corridor. Mice were trained daily for 5 consecutive days to walk down the corridor. On training days, each mouse was placed at the beginning of the corridor and the home cage was placed on its side at the other end of the corridor. Once the mouse traversed the length of the corridor to the home cage, it was allowed to remain for at least 5 minutes before the next training trial. Three training trials were conducted on each day. Mouse forepaws were dipped in black ink so that a print would be left on white paper as the mouse traversed the corridor. Strides were measured from the tip of one paw print to the base of the next paw print on the same side. Stride length was measured in instances in

which at least 5 consecutive uninterrupted strides occurred. Average stride length was based on the analysis of at least 15 strides for each mouse.

Open field performance was measured by individually placing each mouse in an opaque Plexiglas box (61 cm × 61 cm) for 5 minutes. The center of the open field was set 15 cm from the each side of the box. The latency to enter the center of the open field, the time spent in the center, and the number of entries into the center were measured.

The forced swim task was performed by placing each mouse in a beaker (diameter 30 cm) filled with water 27°C ±1°C. The time spent struggling, defined as movements in which forelimbs broke the surface of the water, versus floating, defined as minimum movement required to remain afloat, were scored for the first 6 minutes.

The tail suspension task was performed by suspending each mouse from its tail at a height of 15 cm above a surface. Struggling was defined as forelimb and hindlimb movement or twisting movements. Mice were considered to be immobile if their forelimb and hindlimbs were not moving. Swinging was not scored as movement. Behavior was scored for the first 6 minutes.

The novel object recognition task was conducted as we previously described (Papale et al., 2010). Briefly, mice were acclimated to an open-field box for 10 minutes each day for five consecutive days. On the sixth day each animal was placed in the open-field for 5 minutes and then returned to the home cage for 2 minutes. Mice were then returned to the open field where they were given 5 minutes to explore three objects placed in three of the four corners of the box, at least 10 inches from the edges. Mice were returned to their home cage for either 5 or 20 minutes. Mice were then returned to the open-field for 5 minutes where one object had changed position (novel location), one object had been exchanged for a different object (novel object), and one object was the same (familiar object). The time spent exploring each object during the second exposure was recorded.

Video recordings of open field, forced swim, tail suspension, and novel object recognition tasks were analyzed using Any-Maze video tracking software (Stoelting Co. IL).

The elevated-plus maze consisted of four 30 cm arms (two open and two enclosed), suspended 76 inches above the floor. The test began with the mouse oriented towards an open arm. Each mouse was given 5 minutes to freely explore the apparatus during which time beam breaks were recorded to track movement and location. The percentage of time spent in the open arms was recorded and used as a measure of anxiety as mice naturally prefer the enclosed arms and anxiolytics have been shown to increase the time rodents spend in the open arm (Pellow et al., 1985). The percentage of time spent exploring the open arms was calculated by dividing the time spent in the open arms by the combined time spent in the open and closed arms. Total distance traveled in the apparatus was also recorded.

Sucrose preference was assessed by providing two food cups to each individually housed mouse. One cup contained between 1–2 g of standard rodent diet (Purina, Lab Diet 5001) the second cup contained 1–2 g of high sucrose diet (AIN-76A Rodent Tablets, TestDiet). The amounts of the high sucrose and standard diets consumed over a 1 hour period was

determined by subtracting the post-feeding weight of the food from the pre-feeding weight of the food. This procedure was repeated on 3 consecutive days. The reported sucrose preference values were determined on the third day.

The Y-maze task was performed by placing each mouse at the end of one arm of the Y-maze and allowing free exploration of the apparatus for 8 minutes. The Y-maze consists of three identical arms and a center zone. Spontaneous alternations were recorded.

Continuous video-electrocorticogram (EEG) monitoring

Video-EEG recordings to detect cortical seizure activity were collected and analyzed as we previously described (Dutton et al., 2012; Martin et al., 2007; Papale et al., 2009). EEG recordings from the inferior colliculus were collected as follows. Mice were anesthetized with isoflurane (2-chloro-2-(difluoromethoxy)-1,1,1-trifluoro-thane). Two sterile 0–80×3/32 sterile screw electrodes (Vintage Machine Supplies, Medina, OH) were implanted in the skull at the following coordinates from Bregma (anteroposterior (AP) 1.5 mm and mediolateral (ML) 1.2 mm; AP 1.0 mm and ML 1.2 mm). Stainless steel depth electrodes (diameter 0.25 mm, length 1.5 mm; Plastics One, Roanoke, VA) were implanted at the following coordinates (AP –3.5 mm, ML ±1.5 mm, depth 1.2 mm from the surface of the skull). Two fine-wire electrodes were implanted in the neck muscle for electromyography (EMG) acquisition. Electrodes were covered with dental acrylic following implantation. After a minimum of five days for recovery from surgery, mice were placed in the recording chamber and connected to the EEG acquisition system via a flexible tether and commutator (Dragonfly inc.). Animals were allowed to freely move and were provided food and water *ad libitum*. EEG recordings were sampled at 200 Hz. Signals were digitized, amplified and processed by Stellate Harmonie EEG system (Natus Medical, Inc.). EEG traces were manually scored as previously described (Papale et al., 2013).

Seizure induction

Flurothyl seizure induction was performed as we previously described (Martin et al., 2007). Latencies to the first myoclonic jerk (MJ) and generalized tonic-clonic seizure (GTCS) were recorded. The MJ presents as a jerk of the upper body sometimes accompanied by tail-limb clonus. The GTCS was defined by complete loss of postural control and clonus of all limbs. Mice were also observed for the presence of hindlimb extension immediately following the GTCS.

Partial psychomotor seizures were evoked using the 6 Hz paradigm. Briefly, mice were administered a corneal analgesic 30 minutes prior to stimulation. Corneal electrical stimulation (6-Hz, 3 sec, 14 mA to 30 mA) was applied. Resulting seizures were scored according to the following modified Racine scale: 1 = staring, 2 = forelimb clonus, 3 = rearing and falling.

Audiogenic seizures were examined following auditory stimulation using either key ringing or a high-intensity tone. For the key ringing method, each mouse was placed in a clear Plexiglas box and keys were shaken for 5 minutes approximately 25 cm above the mouse. Shaking a key bundle was found to produce a broad-spectrum acoustic stimulus (13–85

kHz) at an intensity ranging from 50–80 dB, as determined by a 1/4" Brüel & Kjaer microphone (Brüel & Kjaer, Denmark). For the high-intensity tone method, a wide range speaker (Model RT1.3, HiVi inc., Arcadia, CA) was used to produce a 12 kHz, 80 dB tone. Each mouse was exposed to this tone for 5 min. Audiogenic seizures were defined by wild-running behavior progressing to loss of posture and forelimb and hindlimb clonus, sometimes followed by tonic hindlimb extension.

Electrophysiology

Mice P16–28 were deeply anesthetized with halothane, rapidly decapitated, and their brains were removed. Horizontal hippocampal slices were cut 350 μm thick with a vibratome (VT1000S; Leica Systems, Germany) in ice-cold sucrose-containing artificial cerebrospinal fluid (sACSF) (in mM: 85 NaCl, 75 sucrose, 2.5 KCl, 25 glucose, 1.25 NaH_2PO_4 , 4 MgCl_2 , 0.5 CaCl_2 , and 24 NaHCO_3). Slices were incubated in oxygenated normal ACSF (in mM: 126 NaCl, 2.5 KCl, 26 NaHCO_3 , 2 CaCl_2 , 2 MgCl_2 , 1.25 NaH_2PO_4 , and 10 glucose) for 30 minutes to 1 hour at 27°C. All solutions used in preparation and recording were oxygenated by bubbling 95% O_2 –5% CO_2 .

Current clamp recordings were obtained using a MultiClamp 700B amplifier (Molecular Devices, Union City, CA), digitized with a Digidata 1322A digitizer (Molecular Devices), and data were acquired and analyzed with pClamp 10.2 software (Molecular Devices). Signals were sampled at 25 kHz and filtered at 10 kHz. The pipette solution contained the following (in mM): 126 K-gluconate, 4 KCl, 10 HEPES, 4 Mg-ATP, 0.3 Tris-GTP, and 10 Phospho-creatine, pH 7.2. The bath solution contained the following (in mM): 126 NaCl, 1.25 NaH_2PO_4 , 2.5 KCl, 2 CaCl_2 , 2 MgCl_2 , 26 NaHCO_3 , and 10 glucose, pH 7.3. Whole-cell recordings were obtained with access resistance $<25\ \text{M}\Omega$, and cells were held at $-70\ \text{mV}$ for all experiments. Cells were visualized using infrared DIC illumination under 40x magnification. Hyperpolarizing current injections of $-10\ \text{pA}$ and $-30\ \text{pA}$ were used to calculate cellular impedance. Firing patterns were recorded in response to 2-second depolarizing current injections in 20-pA increments, starting at 10 pA, up to 350 pA.

Field recordings were performed as previously described (Makinson et al., 2014). Slices were held at 33°C and perfused (at 2 mL/min) with oxygenated ACSF containing reduced Mg^{++} , 0.5 mM. Recording pipettes (2–3 $\text{M}\Omega$) were pulled from borosilicate glass with a P-87 Flaming-Brown puller (Sutter Instruments, Novato, CA). Electrophysiological recordings were performed using a MultiClamp 700B amplifier (Molecular Devices, Union City, CA) and a Digidata 1322A digitizer (Molecular Devices). Data were acquired and analyzed with pClamp 10.2 software (Molecular Devices). Pipettes were filled with 150 mM NaCl and positioned in the CA3 stratum pyramidale layer. ACSF with elevated potassium was prepared by supplementing standard ACSF with 3 M KCl to raise the potassium concentration to 8.5 mM. The experimental paradigm consisted of a control recording for 2 min in standard ACSF, followed by 15–25 min with 8.5 mM K^+ ACSF perfusion, during which burst activity was recorded. This was followed by a 7-minute washout with standard ACSF. Population spikes were elicited in the CA3 pyramidal layer by stimulation of the mossy fiber tract with a tungsten wire. Population spikes were evoked in physiological 2.5 mM $[\text{K}^+]_0$ before and after exposing the slice to 8.5 mM $[\text{K}^+]_0$. Slices in which population

spike amplitudes did not change more than 20% after exposing the slice to 8.5 mM $[K^+]_O$ were used for analysis.

Auditory Brainstem Nuclei Response

Mice were anesthetized with ketamine and xylazine (i.p., 100 and 10 mg/kg respectively) and placed in a heated (25°C) sound attenuating booth (Industrial Acoustics Company, Bronx, NY). Auditory brainstem responses (ABRs) were recorded using Tucker Davis Technologies BioSigRP© software running on a System 3 platform equipped with an RX5 Pentusa Base Station connected to subdermal electrodes via an RA4LI low impedance headstage (TDT, Alachua, FL, USA). Sets of tone pips at different frequencies were presented in a random order to each animal to avoid possible ordering effects.

A subdermal needle electrode was placed over the skull vertex as the active lead. The ground was placed ventral lateral to the left external pinna and the reference was placed ventral lateral to the right external pinna. The bioelectric signals were sampled at 25 kHz, bandpass filtered between 100 Hz – 3000 Hz, amplified 200,000 times and averaged over 500 consecutive responses, following a previously established ABR screening protocol in mice (Zheng et al., 1999). To determine the ABR threshold, we reduced the stimulus intensity in 10 dB steps and then 5 dB steps until the lowest intensity at which the dominant ABR wave was visible.

Auditory stimuli

Calibrated stimuli were generated using TDT SigGenRP© software and presented through BioSigRP© software via a TDT RX6 digital signal processor at a sample rate of 195 kS/s. Sounds were attenuated by a TDT PA5 programmable attenuator and played from an Infinity EMIT tweeter placed 90° to the right side of the animal. Absolute sound pressure levels (SPL) of sound stimuli were measured prior to ABR recording experiments using a calibrated ¼” Bruel and Kjaer (B&K, Denmark) Type 4139 microphone with a Type 2669 preamplifier. Pure tone pips of 3 ms duration with 1.5 ms cos² rise/fall times were presented for 5, 8, 10, 12, 15, and 24 kHz at a rate of 21 per second.

Immunohistochemistry

Following auditory stimulation, mice were transcardially perfused with ice-cold 4% paraformaldehyde (PFA). Brains were extracted and stored in 30% sucrose for 5 days before slicing. Coronal slices (45 µm) were cut using a cryostat (Leica, Germany). Every fifth slice was washed in phosphate buffered saline (PBS) and incubated overnight in primary rabbit anti-c-Fos antibody (Abcam, 1:5,000). Slices were washed in PBS and incubated in horseradish peroxidase conjugated goat anti-rabbit secondary antibody (GE, 1:5,000) for 30 minutes. Staining was performed using the Vectastain Elite ABC System (Vector). Images were collected and stereological analysis performed using the Microbrightfield stereology system (MBF Bioscience, Williston, VT).

Statistics

All behavioral tests and latencies to flurothyl-induced seizures were analyzed using a one-way analysis of variance (ANOVA) followed by Dunnett’s or Tukey’s *post hoc* tests. Binary

seizure outcomes were analyzed using the χ^2 test. Weight data was analyzed using a two-way analysis of variance, genotype X time. ABRs were analyzed by two-way ANOVA or by the Student's *t-test*. Electrophysiology results were analyzed by Student's *t-test* or ANOVA (one or two-way) followed by Dunn's or Holm-Sidak correction.

RESULTS

The R1627H mutation alters recovery from inactivation, use-dependent inactivation, and persistent current

The effects of a mutation may not be the same in two different VGSCs either because the mutation has different effects on the biophysical properties of the two channels, or because the channels have different physiological functions. To determine how the R1627H mutation altered the properties of Na_v1.6 channels, WT and mutant channels were first expressed in *Xenopus* oocytes and examined by two-electrode voltage clamping. The channels were expressed with the β 1 subunit because β 1 might differentially modulate WT and mutant channels, as we and others have previously observed for mutations that cause GEFS+ (Spampanato et al., 2004). Sample sodium current traces through WT *Scn8a* and R1627H channels are shown in Fig. 1A and B, respectively. The R1627H mutation altered a number of properties in the presence of β 1.

Mutant channels demonstrated a significantly more depolarized $V_{1/2}$ of activation ($-15\pm 1\text{mV}$) compared to WT channels ($-20\pm 2\text{mV}$) (Student's *t-test*, $P < 0.05$, $n = 5$ per group, Fig. 1C). The mutation also led to faster recovery from inactivation (Fig. 1D) and decreased use-dependent inactivation (Fig. 1F), which correlates with faster recovery and increased persistent current (two-way ANOVA, $P < 0.05$, Fig. 1E). The biophysical changes caused by R1627H in Na_v1.6 are predicted to have variable effects on neuronal excitability, with the positive shift in voltage-dependence leading to a decrease in excitability and the faster recovery from inactivation and increased persistent current leading to an increase in excitability.

Targeted knock-in of the R1627H mutation into the mouse *Scn8a* gene

To determine the effects of the R1627H mutation in neurons and on the animal, we generated a mouse model by knocking in the human *SCN1A* R1648H GEFS+ mutation into the corresponding position (R1627) of the mouse *Scn8a* gene. Western blotting was performed on whole brain membrane enriched samples from homozygous *Scn8a*^{RH/RH}, heterozygous *Scn8a*^{RH/+}, and WT littermates ($n = 3$ per genotype). Protein levels of Na_v1.1, Na_v1.2, Na_v1.3, and Na_v1.6 were found to be comparable between WT, *Scn8a*^{RH/+} and *Scn8a*^{RH/RH} littermates, indicating that knock-in of the R1627H mutation did not lead to altered VGSC protein levels (Supplemental Fig. 1).

Survival, weight, and video monitoring of the R1627H line

Mice were monitored and weighed weekly from P10 to P120 to examine locomotor function and to make general assessments of health and survival. R1627H mice were born in approximately the expected Mendelian ratio (1:2:1) (WT = 24, *Scn8a*^{RH/+} = 36, *Scn8a*^{RH/RH} = 28) and had a normal lifespan. However, homozygous *Scn8a*^{RH/RH} mutants gained weight

more slowly so that by 14 weeks of age the average weights of male and female *Scn8a*^{RH/RH} mice were 5.6% (males) and 9.5% (females) less than WT and *Scn8a*^{RH/+} sex-matched littermates, respectively (two-way ANOVA, $P < 0.05$, $n = 11-18$). While WT and *Scn8a*^{RH/+} mice appeared visibly normal, tremors and uncoordinated gait were observed in *Scn8a*^{RH/RH} mutants by the third postnatal week and persisted throughout the life of the animal. The hind legs of *Scn8a*^{RH/RH} mice were rotated outward, possibly to provide a wider base for postural support, and repetitive “high stepping” movements often preceded locomotion. These findings are consistent with recessive motor abnormalities that have been reported in other *Scn8a* mutant mouse lines (Kohrman et al., 1996; Sprunger et al., 1999).

***Scn8a*^{RH/RH} mutant mice have reduced motor function**

Recessive motor dysfunction has been described in other mouse models of *Scn8a* dysfunction. Therefore, we tested whether the *Scn8a*-R1627H mutation also results in altered motor function, even though we did not observe any motor abnormalities in mice with the *Scn1a* R1648H mutation (Martin et al., 2010). Motor function was assessed by measuring 24 hr locomotor activity, rotarod performance, and stride length. Significantly reduced locomotor activity was observed in *Scn8a*^{RH/RH} mice compared to *Scn8a*^{RH/+} and WT littermates in the first 5 hours of the recording period and at the beginning of the dark cycle, when mice are most active (two-way ANOVA, genotype X time, $P < 0.05$, $n = 9-12$, Fig. 2A). Average latency to fall from the rotarod was not significantly different between WT and *Scn8a*^{RH/+}; however, significantly reduced latencies were observed in *Scn8a*^{RH/RH} mutants (one-way ANOVA, $P < 0.05$, $n = 7-18$, Fig. 2B). Shorter stride lengths were also observed in *Scn8a*^{RH/RH} mice when compared to *Scn8a*^{RH/+} and WT littermates (one-way ANOVA, $P < 0.001$, $n = 6-10$, Fig. 2C-D).

The R1627H mutation is not associated with alterations in anxiety, depressive-like behavior, or learning and memory

Scn8a mutations have been associated with alterations in anxiety in mice (McKinney et al., 2008; Sawyer et al., 2014) and psychiatric and cognitive deficits in humans (Trudeau et al., 2006; Wang et al., 2008; Wasserman et al., 2005). However, anxiety levels, as measured by the percentage of time spent in the open arm or the number of entries into the open arm of an elevated plus maze, were comparable between *Scn8a*^{RH/+}, *Scn8a*^{RH/RH} and WT littermates (Table 1). Likewise, no significant differences were observed between the three genotypes in the time spent in the center zone or the number of entries into the center of the open field (Table 1). In the tail suspension task, *Scn8a*^{RH/RH} mice spent significantly more time struggling and less time immobile, when compared to *Scn8a*^{RH/+} and WT littermates (one-way ANOVA, $P < 0.05$, $n = 8-10$); however, no differences in time spent struggling or floating were observed in the forced swim task (one-way ANOVA, $P > 0.05$, $n = 10$ per group, Table 1). Likewise, preference for sucrose was comparable between *Scn8a*^{RH/RH}, *Scn8a*^{RH/+} and WT littermates (one-way ANOVA, $P > 0.05$, $n = 8-12$, Table 1), providing no evidence for depressive-like behavior in the mutant mice.

We previously reported modest improvement in spatial memory in mice with the *Scn8a*^{medjo} mutation (Papale et al., 2010). However, mice carrying the R1627H mutation were found to perform comparably to WT littermates in the novel object recognition task (one-way

ANOVA, $P > 0.05$, $n = 8-12$, Table 1). Spatial learning was also comparable between the three genotypes according to performance in the Y-maze task (one-way ANOVA, $P > 0.05$, $n = 10-12$, Table 1).

Scn8a^{RH/RH} and Scn8a^{RH/+} mice do not exhibit spontaneous seizures

We previously observed spontaneous absence seizures in three *Scn8a* mouse lines (Papale et al., 2009). To determine if the R1627H mutation also leads to seizure generation, ten days of continuous video-EEG recordings were collected from WT, *Scn8a^{RH/+}*, and *Scn8a^{RH/RH}* mice. No seizures were detected in any mice ($n = 4-6$). Based on previous work, the C3H/HeJ genetic background is known to be more permissive to the generation of absence seizures (Beyer et al., 2008). Therefore, we crossed *Scn8a^{RH/+}* mice to the C3H/HeJ background for five generations and then repeated the EEG analysis. No absence seizures were observed over five days of continuous video-EEG recordings collected from *Scn8a^{RH/+}* mutants and WT littermates at this generation ($n = 5-6$).

Scn8a^{RH/+} but not Scn8a^{RH/RH} mice are resistant to 6 Hz- and flurothyl-induced seizures

Average latency to the flurothyl-induced myoclonic jerk (MJ) and the generalized tonic-clonic seizure (GTCS) were significantly increased in *Scn8a^{RH/+}* mice when compared to *Scn8a^{RH/RH}* and WT littermates (one-way ANOVA, $P < 0.05$, Fig. 3A). However, the severity of the seizures, as assessed by the presence of hindlimb extension and mortality following the GTCS, was reduced in both *Scn8a^{RH/+}* and *Scn8a^{RH/RH}* mice when compared to WT littermates (χ^2 , $P < 0.05$, Fig. 3B). Similarly, *Scn8a^{RH/+}* but not *Scn8a^{RH/RH}* mice were found to be resistant to 6 Hz-induced psychomotor seizures when compared to WT littermates (Fig. 3C), and the severity of the observed 6 Hz-induced seizures was lower in both *Scn8a^{RH/+}* and *Scn8a^{RH/RH}* mice when compared to WT littermates at current intensities of 20, 22, and 24 mA (one-way ANOVA, $P < 0.0001$, Dunnett's *post hoc*, $P < 0.001$, Fig. 3D).

Scn8a mutant mice have reduced hippocampal bursting activity in the presence of high extracellular potassium

To examine the susceptibility of the CNS network to seizure-like activity, extracellular recordings were performed in the CA3 region of hippocampal slices from WT, *Scn8a^{RH/+}* and *Scn8a^{RH/RH}* mice in the presence of high extracellular potassium (Fig. 4A). We previously observed reduced hippocampal bursting in *Scn8a^{med/+}* mice that carry a loss of function *Scn8a* mutation using the high [K⁺] seizure model (Makinson et al., 2014) and reduced hippocampal network excitability is thought to be a key component of *Scn8a*-related seizure resistance (Blumenfeld et al., 2009; Makinson et al., 2014). We found that the percentage of slices exhibiting bursting was significantly lower in *Scn8a^{RH/+}* mice (1/8, 12.5%) compared to WT (5/5, 100%) and *Scn8a^{RH/RH}* mice (4/7, 57.1%) (Fig. 4B). The average latency to the onset of bursting was comparable between slices from WT mice (6.1 min) and *Scn8a^{RH/RH}* mutants (6.3 min). However slices from *Scn8a^{RH/+}* did not show bursting even upon prolonged (> 20 min) exposure to elevated potassium, except for 1 slice (1/8) that did show bursting with a latency of 20 min (Fig. 4C). The intra-burst spiking frequency was reduced in that one *Scn8a^{RH/+}* slice (32.0 Hz) and also in slices from

Scn8a^{RH/RH} mice (49.3 Hz) when compared to WT slices (61.5 Hz) (Fig. 4D). These results indicate that slices from heterozygous *Scn8a* R1627H mice are resistant to seizure-like activity compared to WT, and slices from homozygous mice are intermediate between heterozygous and WT in their susceptibility to seizure-like activity.

Scn8a mutant mice have altered hippocampal cell firing

Based on oocyte data (Fig. 1), the effects of the R1627H mutation on sodium channel recovery and persistent current would be predicted to increase neuronal activity, whereas the effects on the voltage-dependence of activation would be predicted to decrease activity. Therefore, we examined the effect of the mutation on network excitability by current clamp in hippocampal slices. Consistent with the predictions based on the biophysical properties of the channel in oocytes, the R1627H mutation altered action potential firing in CA3 pyramidal neurons in a complex manner. *Scn8a*^{RH/+} neurons fired more action potentials than WT and *Scn8a*^{RH/RH} neurons, and *Scn8a*^{RH/RH} neurons fired more action potentials than WT. These differences were statistically significant (two-way ANOVA, $P < 0.05$, $n = 21-28$, Fig. 5A–B). The action potential height measured from threshold was significantly decreased in *Scn8a*^{RH/RH} neurons compared to WT and *Scn8a*^{RH/+} (two-way ANOVA, $P < 0.05$, $n = 21-28$, Table 2), and the action potential amplitude half-width was increased (broadened) for both *Scn8a*^{RH/RH} and *Scn8a*^{RH/+} compared to WT (two-way ANOVA, $P < 0.05$, $n = 21-28$, Table 2). The threshold for firing an action potential was slightly higher for the mutants compared to WT, but the differences were not significantly different (two-way ANOVA, $P > 0.05$, $n = 21-28$, Table 2). Overall, pyramidal neurons from *Scn8a*^{RH/+} and *Scn8a*^{RH/RH} mutants demonstrated greater excitability compared to WT. Hippocampal interneurons recorded from sub-pyramidal layers of CA3 in *Scn8a*^{RH/+} mice fired fewer action potentials compared to WT (two-way ANOVA, $P < 0.05$, $n = 6-8$, Fig. 5D), while no significant difference was observed between interneuron firing of *Scn8a*^{RH/RH} and WT neurons. Furthermore, no differences were observed in interneuron action potential properties (two-way ANOVA, $P > 0.05$, $n = 6-8$, Table 2). The resting membrane potentials of pyramidal neurons and interneurons across all genotypes were approximately -70 mV and -65 mV, respectively. There were no significant differences in the cell impedance of pyramidal and inhibitory neurons.

The Scn8a-R1627H mutation increases the lifespan and seizure thresholds of Scn1a-R1648H GEFS+ mice

The R1627H mutation in *Scn8a* is orthologous to the *Scn1a* R1648H mutation that causes GEFS+ in humans. To determine if there is a functional interaction between the two channels with orthologous mutations, we crossed the two lines to generate offspring with the following genotypes: *Scn1a*^{RH/+}, *Scn1a*^{RH/RH}, *Scn8a*^{RH/+}, *Scn1a*^{RH/+}/*Scn8a*^{RH/+}, *Scn1a*^{RH/RH}/*Scn8a*^{RH/+}, and WT. *Scn1a*^{RH/+} and *Scn1a*^{RH/RH} mice experienced 18% (2/11) and 100% (11/11) mortality by 3 months of age, respectively. In contrast, 40% of *Scn1a*^{RH/RH}/*Scn8a*^{RH/+} mutants survived to at least three months of age. No mortality was observed in WT, *Scn8a*^{RH/+}, and *Scn1a*^{RH/+}/*Scn8a*^{RH/+} mice (Fig. 6A). As previously observed, the average latency to the flurothyl-induced GTCS was lower in *Scn1a*^{RH/+} mutants; however, latencies to the GTCS were comparable between *Scn1a*^{RH/+}/*Scn8a*^{RH/+} mutants and WT littermates (Fig. 5B). In contrast, significantly lower latencies to the MJ

and GTCS were still observed in *Scn1a*^{RH/RH}/*Scn8a*^{RH/+} mutants (one-way ANOVA, Dunnett's *post hoc*, *P < 0.05, ***P < 0.001, n = 5–17, Fig. 6B). The increase in lifespan and seizure thresholds is consistent with our previous results examining the interactions between the *Scn8a*^{medjo} and GEFS+ or DS *Scn1a* mutants (Hawkins et al., 2011; Martin et al., 2007).

Scn8a^{RH/RH} mice exhibit wild running behavior in response to high intensity sound stimuli

Scn8a^{RH/RH} mice were sometimes observed exhibiting wild-running in response to elevated sound stimuli. To further explore this behavior, *Scn8a*^{RH/+}, *Scn8a*^{RH/RH}, and WT littermates were exposed to tones (12 kHz, 80 dB) or broad-spectrum (13–85 kHz, 50–80 dB) acoustic stimuli. Approximately 36% (11/31) of *Scn8a*^{RH/RH} mice exhibited wild-running behavior followed by loss of postural control and forelimb and hindlimb clonus in response to sound stimuli (χ^2 , *P < 0.05, Fig. 7A). In contrast, only one WT littermate (1/15, 7%) exhibited wild running behavior in response to the sound stimulus. Furthermore, this WT mouse progressed to tonic hindlimb extension, which was not observed in the *Scn8a*^{RH/RH} mutants. No *Scn8a*^{RH/+} mice (0/10) exhibited abnormal audiogenic responses.

To investigate whether the observed abnormal behaviors may have been the result of audiogenic seizures, we recorded EEG activity in the inferior colliculus, which has been shown to be an important site for the initiation and maintenance of audiogenic seizures (Browning, 1986; Kesner, 1966; Willott and Lu, 1980). EEG activity in *Scn8a*^{RH/RH} mice was unaltered by exposure to the tone prior to the onset of the behavioral response (Fig. 7B). However at the onset of the behavioral response, we observed high amplitude - greater than twice baseline - EEG signals in the inferior colliculus of *Scn8a*^{RH/RH} mice (Fig. 7B). High amplitude EEG activity was not observed in cortical EEG recordings during the sound-induced behavioral response (Fig. 7B). To provide an independent measure of neuronal activity following sound exposure, we performed immunohistochemistry to compare c-Fos expression in the cortex, hippocampus, superior colliculus and inferior colliculus of responding and non-responding *Scn8a*^{RH/RH} mice as well as *Scn8a*^{RH/+} and WT controls (Fig. 7C–E). In agreement with the EEG results, low levels of c-Fos expression was observed in the cortex and hippocampus of all animals (Fig. 7D). High levels of c-Fos expression were observed in the superior and inferior colliculus of responding *Scn8a*^{RH/RH} mice but not non-responding *Scn8a*^{RH/RH}, WT, or *Scn8a*^{RH/+} mice (Fig. 7D).

Scn8a^{RH/RH} mice have reduced auditory brainstem responses (ABRs)

To test the possibility that the sound-induced wild running behavior in *Scn8a*^{RH/RH} mice may have been the result of increased hearing ability, ABRs to sound stimuli were recorded (Fig. 8). WT, *Scn8a*^{RH/+} and *Scn8a*^{RH/RH} mice were exposed to 5–24 kHz tones from 110–20 dB SPL while measuring ABR responses. *Scn8a*^{RH/RH} mice were found to have higher thresholds between 12–15 kHz (two-way ANOVA, genotype X frequency, Dunnett's *post hoc*, *P < 0.05, Fig. 8A,C). However, no differences in ABR thresholds were observed between *Scn8a*^{RH/RH} mice that were not susceptible to sound-induced wild-running behavior (non-responders) and *Scn8a*^{RH/RH} mice that were found to be susceptible (responders) (Student's *t-test*, P > 0.05, Fig. 8B).

DISCUSSION

We constructed a mouse line in which the *SCN1A* GEFS+ mutation R1648H was introduced into the corresponding position in the mouse *Scn8a* gene (R1627H). The biophysical properties of the two sodium channels were altered by the mutation in similar but not identical ways. In oocytes, the R1627H mutation altered some properties of $\text{Na}_v1.6$ function that would be predicted to increase neuronal excitability, including faster recovery from inactivation, reduced use dependence and increased persistent current. These effects are consistent with those previously observed for R1648H (Lossin et al., 2002; Spampinato et al., 2001).

Action potential firing of pyramidal neurons was increased in heterozygous and homozygous R1627H mice compared to WT. These results contrast with our previous investigation of the *Scn1a*-R1648H mutation in which we observed no significant changes in excitability of pyramidal neurons from mutant compared to WT mice (Martin et al., 2010). Because the *Scn1a*-R1648H mutation also markedly decreased action potential firing in inhibitory bipolar neurons (Martin et al., 2010) and *Scn8a* expression has been detected at the axon initial segments of parvalbumin positive interneurons (Lorincz and Nusser, 2008), we also recorded from CA3 interneurons of *Scn8a*-R1627H animals. The only difference we observed in interneuron firing was a decrease in the number of action potentials from heterozygous mutants compared to WT mice. To assess the net effect of the *Scn8a*-R1627H mutation on network excitability, we examined seizure-like activity (bursting) in response to elevated extracellular potassium. Slices from the *Scn8a*^{RH/+} mice exhibited less epileptiform bursting activity (Fig. 4), consistent with increased seizure resistance. Interestingly, no change in the latency to burst onset was observed between *Scn8a*^{RH/RH} compared to WT slices, and more slices from *Scn8a*^{RH/RH} mice displayed bursting behavior compared to *Scn8a*^{RH/+} littermates, indicating a partial loss of seizure resistance at the homozygous level (Fig. 4). Similarly *Scn8a*^{RH/+} but not *Scn8a*^{RH/RH} animals were found to be resistant to flurothyl and electrically induced seizures (Fig. 3). It is not clear if the observed increase in CA3 pyramidal neuron firing and decrease in interneuron firing contributes directly to seizure resistance or if it results from compensatory responses to reduced network excitability in the heterozygous mice.

Consistent with findings from some other *Scn8a* mouse mutants, at the heterozygous level, the R1627H mutation increased resistance to induced seizures and compensated for the increase in seizure susceptibility resulting from the orthologous GEFS+ R1648H mutation in the *Scn1a* gene (Hawkins et al., 2011; Makinson et al., 2014; Martin et al., 2007).

A novel feature of the R1627H mice was their abnormal behavioral response to sound stimuli, which has not been previously reported in *Scn8a* mutants. Three observations suggest that the sound-induced wild running and forelimb-hindlimb clonic events represented audiogenic seizures. First, the behavioral presentation of these events, consisting of loss of posture and forelimb and hindlimb clonus, was similar to flurothyl-induced brainstem seizure behaviors (Samoriski et al., 1998). Second, following exposure to auditory stimuli, *Scn8a*^{RH/RH} mice that exhibited the abnormal behavior expressed high levels of c-Fos expression in the brainstem, including the inferior colliculus, a region responsible for

the initiation and maintenance of audiogenic seizures (Browning, 1986; Kesner, 1966; Willott and Lu, 1980). In contrast, c-Fos expression was not increased in the midbrain and brainstem of non-responding *Scn8a^{RH/RH}*, *Scn8a^{RH/+}*, or WT littermates and comparatively little c-Fos expression was observed outside of brainstem regions in *Scn8a^{RH/RH}* responders following the auditory stimulus. c-Fos expression in brainstem nuclei following exposure to sound stimuli is a hallmark of audiogenic seizures (Klein et al., 2004; Kwon and Pierson, 1997; Le Gal La Salle and Naquet, 1990; Snyder-Keller and Pierson, 1992). Third, we observed increased amplitude of EEG signals in the inferior colliculus during the abnormal behavior in *Scn8a^{RH/RH}* mice, indicating hypersynchronous neuronal activity in a major audiogenic seizure region. *Scn8a^{RH/RH}* mice were also found to have higher ABR thresholds. This was similarly observed in the *Scn8a* mutant ‘Cloth-ears’, lending further support to the prediction that *Scn8a* dysfunction may contribute to neural hearing loss (Mackenzie et al., 2009).

Homozygous *Scn8a^{RH/RH}* mutants exhibited motor impairments and reduced locomotor activity, consistent with previously described *Scn8a* rodent models (Dickie, 1965; Hamann et al., 2003; Kearney et al., 2002; Kohrman et al., 1996). However, in contrast to previously described *Scn8a* mutants, R1627H mutants did not display alterations in measures of anxiety, or learning and memory (McKinney et al., 2008; Papale et al., 2010).

Unexpectedly, R1627H mutants did not exhibit absence seizures, which were observed in mice expressing *Scn8a^{8J}*, *Scn8a^{med}*, and *Scn8a^{medjo}* alleles (Papale et al., 2009). Across measurements of seizure susceptibility, the R1627H mutants contrast strikingly to the severe convulsive seizures and premature lethality observed in mice expressing the epileptic encephalopathy *SCN8A* N1768D mutation (Wagnon et al., 2014). Since electrophysiological analysis of neurons from *Scn8a* N1768D mutants has not yet been reported, a more direct comparison of the effect of each mutation on neuronal excitability cannot be performed. However, the striking phenotypic differences between these two mutants highlight the importance of studying mouse lines expressing different *SCN8A* mutations.

CONCLUSIONS

The increased seizure resistance conferred by the *Scn8a* R1627H mutation at the heterozygous level raises the possibility that seizure protection may be achieved by targeting specific biophysical properties of *Scn8a* function without elevating the risk of spontaneous seizure generation or negative behavioral outcomes. However, we report that the seizure resistance of the R1627H mutation was lost at the homozygous level and that these mice additionally were susceptible to audiogenic seizures, which coincided with increased pyramidal cell excitability but normal interneuron excitability. Together these observations indicate that *Scn8a* is an important regulator of excitatory as well as inhibitory cell excitability. This study expands upon the phenotypes associated with disruption of the *Scn8a* gene and demonstrates that an *Scn8a* mutation can both confer seizure protection and increase seizure susceptibility.

Supplementary Material

Refer to Web version on PubMed Central for supplementary material.

Acknowledgments

We would like to thank Dr. David Weinshenker and Dr. Jason Schroeder of the Emory University Rodent Behavioral Core for assistance with assessing locomotor activity.

Research in this publication was supported by the National Institute of Neurological Disorders and Stroke (NINDS) and National Institute on Deafness and Communication Disorders (NIDCD) of the National Institutes of Health (NIH) under award numbers R01NS072221 (A.E.), R01NS048336 (A.L.G.), R01NS065187 (A.E. and A.L.G.), F31NS074717 (C.D.M), and R01DC008343 (R.L).

References

- Beyer B, Deleuze C, Letts VA, Mahaffey CL, Boumil RM, Lew TA, Huguenard JR, Frankel WN. Absence seizures in C3H/HeJ and knockout mice caused by mutation of the AMPA receptor subunit Gria4. *Human molecular genetics*. 2008; 17:1738–1749. [PubMed: 18316356]
- Blumenfeld H, Lampert A, Klein JP, Mission J, Chen MC, Rivera M, Dib-Hajj S, Brennan AR, Hains BC, Waxman SG. Role of hippocampal sodium channel Nav1.6 in kindling epileptogenesis. *Epilepsia*. 2009; 50:44–55. [PubMed: 18637833]
- Browning RA. Neuroanatomical localization of structures responsible for seizures in the GEPR: lesion studies. *Life sciences*. 1986; 39:857–867. [PubMed: 3747710]
- Carvill GL, Heavin SB, Yendle SC, McMahon JM, O’Roak BJ, Cook J, Khan A, Dorschner MO, Weaver M, Calvert S, Malone S, Wallace G, Stanley T, Bye AM, Bleasel A, Howell KB, Kivity S, Mackay MT, Rodriguez-Casero V, Webster R, Korczyn A, Afawi Z, Zelnick N, Lerman-Sagie T, Lev D, Moller RS, Gill D, Andrade DM, Freeman JL, Sadleir LG, Shendure J, Berkovic SF, Scheffer IE, Mefford HC. Targeted resequencing in epileptic encephalopathies identifies de novo mutations in CHD2 and SYNGAP1. *Nature genetics*. 2013; 45:825–830. [PubMed: 23708187]
- Claes L, Del-Favero J, Ceulemans B, Lagae L, Van Broeckhoven C, De Jonghe P. De novo mutations in the sodium-channel gene SCN1A cause severe myoclonic epilepsy of infancy. *American journal of human genetics*. 2001; 68:1327–1332. [PubMed: 11359211]
- Claes LR, Deprez L, Suls A, Baets J, Smets K, Van Dyck T, Deconinck T, Jordanova A, De Jonghe P. The SCN1A variant database: a novel research and diagnostic tool. *Human mutation*. 2009; 30:E904–920. [PubMed: 19585586]
- de Kovel CG, Meisler MH, Brilstra EH, van Berkestijn FM, Slot RV, van Lieshout S, Nijman IJ, O’Brien JE, Hammer MF, Estacion M, Waxman SG, Dib-Hajj SD, Koeleman BP. Characterization of a de novo SCN8A mutation in a patient with epileptic encephalopathy. *Epilepsy research*. 2014; 108:1511–1518. [PubMed: 25239001]
- Dickie MM. Jolting. *Mouse News Lett*. 1965; 32:44.
- Dutton SB, Makinson CD, Papale LA, Shankar A, Balakrishnan B, Nakazawa K, Escayg A. Preferential inactivation of *Scn1a* in parvalbumin interneurons increases seizure susceptibility. *Neurobiology of disease*. 2012; 49C:211–220. [PubMed: 22926190]
- Escayg A, Goldin AL. Sodium channel SCN1A and epilepsy: mutations and mechanisms. *Epilepsia*. 2010; 51:1650–1658. [PubMed: 20831750]
- Escayg A, MacDonald BT, Meisler MH, Baulac S, Huberfeld G, An-Gourfinkel I, Brice A, LeGuern E, Moulard B, Chaigne D, Buresi C, Malafosse A. Mutations of SCN1A, encoding a neuronal sodium channel, in two families with GEFS+2. *Nature genetics*. 2000; 24:343–345. [PubMed: 10742094]
- Estacion M, Gasser A, Dib-Hajj SD, Waxman SG. A sodium channel mutation linked to epilepsy increases ramp and persistent current of Nav1.3 and induces hyperexcitability in hippocampal neurons. *Experimental neurology*. 2010; 224:362–368. [PubMed: 20420834]

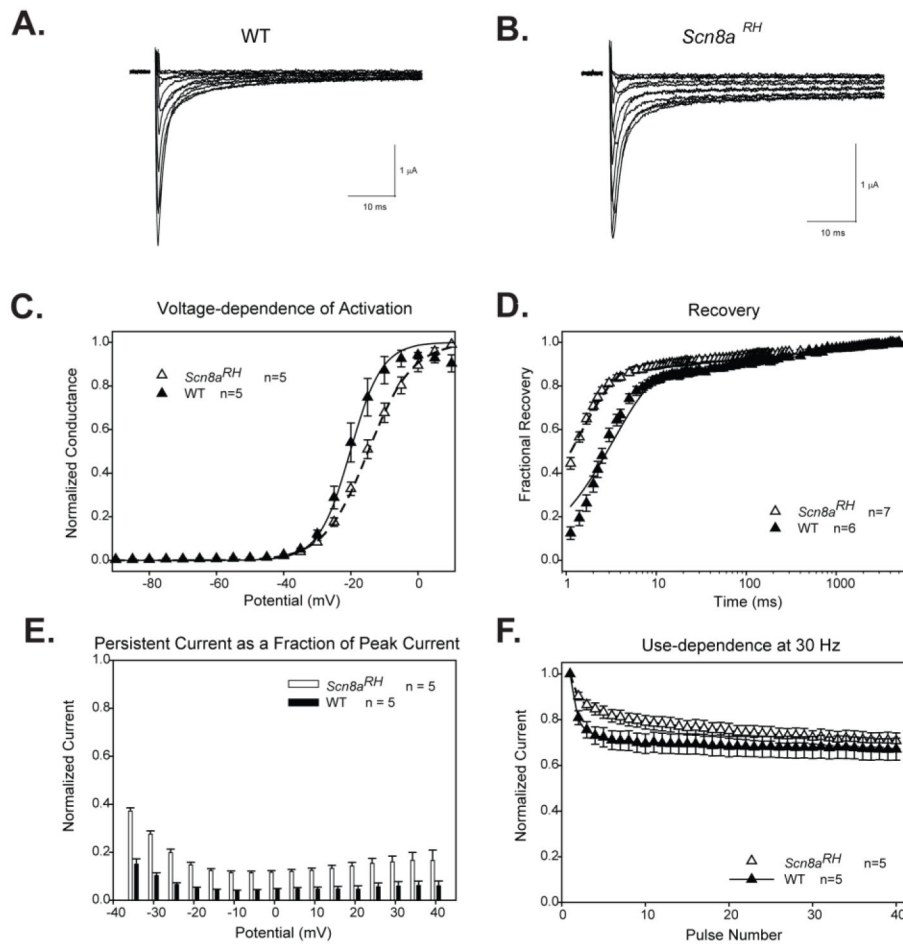
- Estacion M, O'Brien JE, Conravey A, Hammer MF, Waxman SG, Dib-Hajj SD, Meisler MH. A novel de novo mutation of SCN8A (Nav1.6) with enhanced channel activation in a child with epileptic encephalopathy. *Neurobiology of disease*. 2014; 69:117–123. [PubMed: 24874546]
- Hamann M, Meisler MH, Richter A. Motor disturbances in mice with deficiency of the sodium channel gene *Scn8a* show features of human dystonia. *Experimental neurology*. 2003; 184:830–838. [PubMed: 14769375]
- Hawkins NA, Martin MS, Frankel WN, Kearney JA, Escayg A. Neuronal voltage-gated ion channels are genetic modifiers of generalized epilepsy with febrile seizures plus. *Neurobiology of disease*. 2011; 41:655–660. [PubMed: 21156207]
- Heron SE, Crossland KM, Andermann E, Phillips HA, Hall AJ, Bleasel A, Shevell M, Mercho S, Seni MH, Guiot MC, Mulley JC, Berkovic SF, Scheffer IE. Sodium-channel defects in benign familial neonatal-infantile seizures. *Lancet*. 2002; 360:851–852. [PubMed: 12243921]
- Holland KD, Kearney JA, Glauser TA, Buck G, Keddache M, Blankston JR, Glauser IW, Kass RS, Meisler MH. Mutation of sodium channel SCN3A in a patient with cryptogenic pediatric partial epilepsy. *Neuroscience letters*. 2008; 433:65–70. [PubMed: 18242854]
- Kearney JA, Buchner DA, De Haan G, Adamska M, Levin SI, Furay AR, Albin RL, Jones JM, Montal M, Stevens MJ, Sprunger LK, Meisler MH. Molecular and pathological effects of a modifier gene on deficiency of the sodium channel *Scn8a* (Nav1.6). *Human molecular genetics*. 2002; 11:2765–2775. [PubMed: 12374766]
- Kesner RP. Subcortical mechanisms of audiogenic seizures. *Experimental neurology*. 1966; 15:192–205. [PubMed: 4951856]
- Klein BD, Fu YH, Ptacek LJ, White HS. c-Fos immunohistochemical mapping of the audiogenic seizure network and tonotopic neuronal hyperexcitability in the inferior colliculus of the Frings mouse. *Epilepsy research*. 2004; 62:13–25. [PubMed: 15519128]
- Kohrman DC, Smith MR, Goldin AL, Harris J, Meisler MH. A missense mutation in the sodium channel *Scn8a* is responsible for cerebellar ataxia in the mouse mutant jolting. *The Journal of neuroscience : the official journal of the Society for Neuroscience*. 1996; 16:5993–5999. [PubMed: 8815882]
- Kwon J, Pierson M. Fos-immunoreactive responses in inferior colliculi of rats with experimental audiogenic seizure susceptibility. *Epilepsy research*. 1997; 27:89–99. [PubMed: 9192183]
- Le Gal La Salle G, Naquet R. Audiogenic seizures evoked in DBA/2 mice induce c-fos oncogene expression into subcortical auditory nuclei. *Brain research*. 1990; 518:308–312. [PubMed: 2117990]
- Lorincz A, Nusser Z. Cell-type-dependent molecular composition of the axon initial segment. *The Journal of neuroscience : the official journal of the Society for Neuroscience*. 2008; 28:14329–14340. [PubMed: 19118165]
- Lossin C. A catalog of SCN1A variants. *Brain & development*. 2009; 31:114–130. [PubMed: 18804930]
- Lossin C, Wang DW, Rhodes TH, Vanoye CG, George AL Jr. Molecular basis of an inherited epilepsy. *Neuron*. 2002; 34:877–884. [PubMed: 12086636]
- Mackenzie FE, Parker A, Parkinson NJ, Oliver PL, Brooker D, Underhill P, Lukashkina VA, Lukashkin AN, Holmes C, Brown SD. Analysis of the mouse mutant Cloth-ears shows a role for the voltage-gated sodium channel *Scn8a* in peripheral neural hearing loss. *Genes, brain, and behavior*. 2009; 8:699–713.
- Makinson CD, Tanaka BS, Lamar T, Goldin AL, Escayg A. Role of the hippocampus in Nav1.6 (*Scn8a*) mediated seizure resistance. *Neurobiology of disease*. 2014; 68:16–25. [PubMed: 24704313]
- Martin MS, Dutt K, Papale LA, Dube CM, Dutton SB, de Haan G, Shankar A, Tufik S, Meisler MH, Baram TZ, Goldin AL, Escayg A. Altered function of the SCN1A voltage-gated sodium channel leads to gamma-aminobutyric acid-ergic (GABAergic) interneuron abnormalities. *The Journal of biological chemistry*. 2010; 285:9823–9834. [PubMed: 20100831]
- Martin MS, Tang B, Papale LA, Yu FH, Catterall WA, Escayg A. The voltage-gated sodium channel *Scn8a* is a genetic modifier of severe myoclonic epilepsy of infancy. *Human molecular genetics*. 2007; 16:2892–2899. [PubMed: 17881658]

- McKinney BC, Chow CY, Meisler MH, Murphy GG. Exaggerated emotional behavior in mice heterozygous null for the sodium channel *Scn8a* (*Nav1.6*). *Genes, brain, and behavior*. 2008; 7:629–638.
- O'Brien JE, Meisler MH. Sodium channel *SCN8A* (*Nav1.6*): properties and de novo mutations in epileptic encephalopathy and intellectual disability. *Frontiers in genetics*. 2013; 4:213. [PubMed: 24194747]
- Papale LA, Beyer B, Jones JM, Sharkey LM, Tufik S, Epstein M, Letts VA, Meisler MH, Frankel WN, Escayg A. Heterozygous mutations of the voltage-gated sodium channel *SCN8A* are associated with spike-wave discharges and absence epilepsy in mice. *Human molecular genetics*. 2009; 18:1633–1641. [PubMed: 19254928]
- Papale LA, Makinson CD, Christopher Ehlen J, Tufik S, Decker MJ, Paul KN, Escayg A. Altered sleep regulation in a mouse model of *SCN1A*-derived genetic epilepsy with febrile seizures plus (*GEFS+*). *Epilepsia*. 2013; 54:625–634. [PubMed: 23311867]
- Papale LA, Paul KN, Sawyer NT, Manns JR, Tufik S, Escayg A. Dysfunction of the *Scn8a* voltage-gated sodium channel alters sleep architecture, reduces diurnal corticosterone levels, and enhances spatial memory. *The Journal of biological chemistry*. 2010; 285:16553–16561. [PubMed: 20353942]
- Pellow S, Chopin P, File SE, Briley M. Validation of open:closed arm entries in an elevated plus-maze as a measure of anxiety in the rat. *Journal of neuroscience methods*. 1985; 14:149–167. [PubMed: 2864480]
- Samoriski GM, Piekut DT, Applegate CD. Regional analysis of the spatial patterns of Fos induction in brain following flurothyl kindling. *Neuroscience*. 1998; 84:1209–1222. [PubMed: 9578407]
- Sawyer NT, Papale LA, Eliason J, Neigh GN, Escayg A. *Scn8a* voltage-gated sodium channel mutation alters seizure and anxiety responses to acute stress. *Psychoneuroendocrinology*. 2014; 39:225–236. [PubMed: 24138934]
- Snyder-Keller AM, Pierson MG. Audiogenic seizures induce c-fos in a model of developmental epilepsy. *Neuroscience letters*. 1992; 135:108–112. [PubMed: 1542426]
- Spampanato J, Escayg A, Meisler MH, Goldin AL. Functional effects of two voltage-gated sodium channel mutations that cause generalized epilepsy with febrile seizures plus type 2. *The Journal of neuroscience : the official journal of the Society for Neuroscience*. 2001; 21:7481–7490. [PubMed: 11567038]
- Spampanato J, Kearney JA, de Haan G, McEwen DP, Escayg A, Aradi I, MacDonald BT, Levin SI, Soltesz I, Benna P, Montalenti E, Isom LL, Goldin AL, Meisler MH. A novel epilepsy mutation in the sodium channel *SCN1A* identifies a cytoplasmic domain for beta subunit interaction. *The Journal of neuroscience : the official journal of the Society for Neuroscience*. 2004; 24:10022–10034. [PubMed: 15525788]
- Sprunger LK, Escayg A, Tallaksen-Greene S, Albin RL, Meisler MH. Dystonia associated with mutation of the neuronal sodium channel *Scn8a* and identification of the modifier locus *Scnm1* on mouse chromosome 3. *Human molecular genetics*. 1999; 8:471–479. [PubMed: 9949206]
- Trudeau MM, Dalton JC, Day JW, Ranum LP, Meisler MH. Heterozygosity for a protein truncation mutation of sodium channel *SCN8A* in a patient with cerebellar atrophy, ataxia, and mental retardation. *Journal of medical genetics*. 2006; 43:527–530. [PubMed: 16236810]
- Vaher U, Noukas M, Nikopentis T, Kals M, Annilo T, Nelis M, Ounap K, Reimand T, Talvik I, Ilves P, Piirsoo A, Seppet E, Metspalu A, Talvik T. De Novo *SCN8A* Mutation Identified by Whole-Exome Sequencing in a Boy With Neonatal Epileptic Encephalopathy, Multiple Congenital Anomalies, and Movement Disorders. *Journal of child neurology*. 2013; 54:1270–1281.
- Vanoye CG, Gurnett CA, Holland KD, George AL Jr, Kearney JA. Novel *SCN3A* variants associated with focal epilepsy in children. *Neurobiology of disease*. 2014; 62:313–322. [PubMed: 24157691]
- Veeramah KR, O'Brien JE, Meisler MH, Cheng X, Dib-Hajj SD, Waxman SG, Talwar D, Girirajan S, Eichler EE, Restifo LL, Erickson RP, Hammer MF. De novo pathogenic *SCN8A* mutation identified by whole-genome sequencing of a family quartet affected by infantile epileptic encephalopathy and SUDEP. *American journal of human genetics*. 2012; 90:502–510. [PubMed: 22365152]

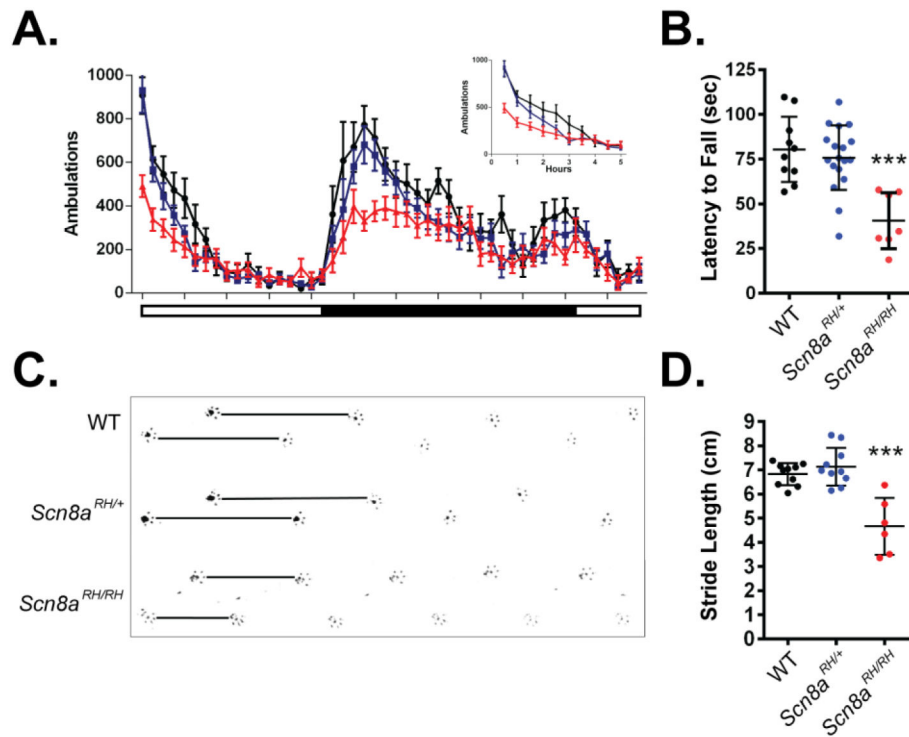
- Wagnon JL, Korn MJ, Parent R, Tarpey TA, Jones JM, Hammer MF, Murphy GG, Parent JM, Meisler MH. Convulsive seizures and SUDEP in a mouse model of SCN8A epileptic encephalopathy. *Human molecular genetics*. 2014
- Wang Y, Zhang J, Li X, Ji J, Yang F, Wan C, Feng G, Wan P, He L, He G. SCN8A as a novel candidate gene associated with bipolar disorder in the Han Chinese population. *Progress in neuro-psychopharmacology & biological psychiatry*. 2008; 32:1902–1904. [PubMed: 18812204]
- Wasserman D, Geijer T, Rozanov V, Wasserman J. Suicide attempt and basic mechanisms in neural conduction: relationships to the SCN8A and VAMP4 genes. *American journal of medical genetics. Part B, Neuropsychiatric genetics : the official publication of the International Society of Psychiatric Genetics*. 2005; 133B:116–119.
- Willott JF, Lu SM. Midbrain pathways of audiogenic seizures in DBA/2 mice. *Experimental neurology*. 1980; 70:288–299. [PubMed: 7428896]
- Yu FH, Mantegazza M, Westenbroek RE, Robbins CA, Kalume F, Burton KA, Spain WJ, McKnight GS, Scheuer T, Catterall WA. Reduced sodium current in GABAergic interneurons in a mouse model of severe myoclonic epilepsy in infancy. *Nature neuroscience*. 2006; 9:1142–1149. [PubMed: 16921370]
- Zheng QY, Johnson KR, Erway LC. Assessment of hearing in 80 inbred strains of mice by ABR threshold analyses. *Hearing research*. 1999; 130:94–107. [PubMed: 10320101]

Highlights

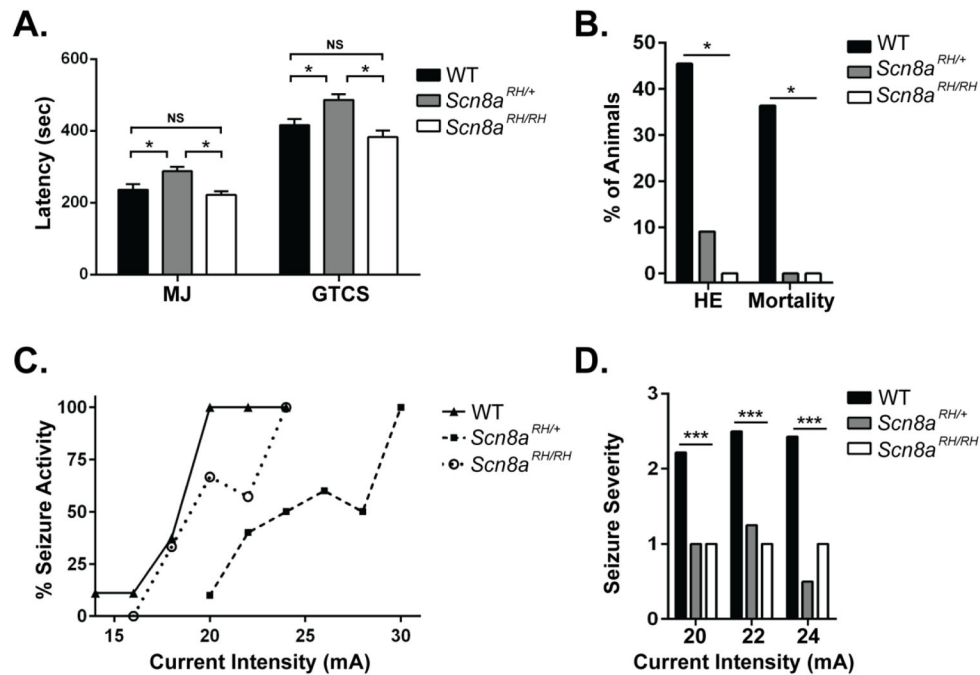
- The R1627H mutation provides seizure resistance without causing absence epilepsy.
- *Scn8a*-dependent seizure phenotypes are gene-dose dependent.
- The R1627H mutation alters excitatory and inhibitory neuronal excitability in the hippocampus.
- The *Scn8a*-R1627H mutation increases susceptibility to audiogenic seizures

**FIGURE 1.**

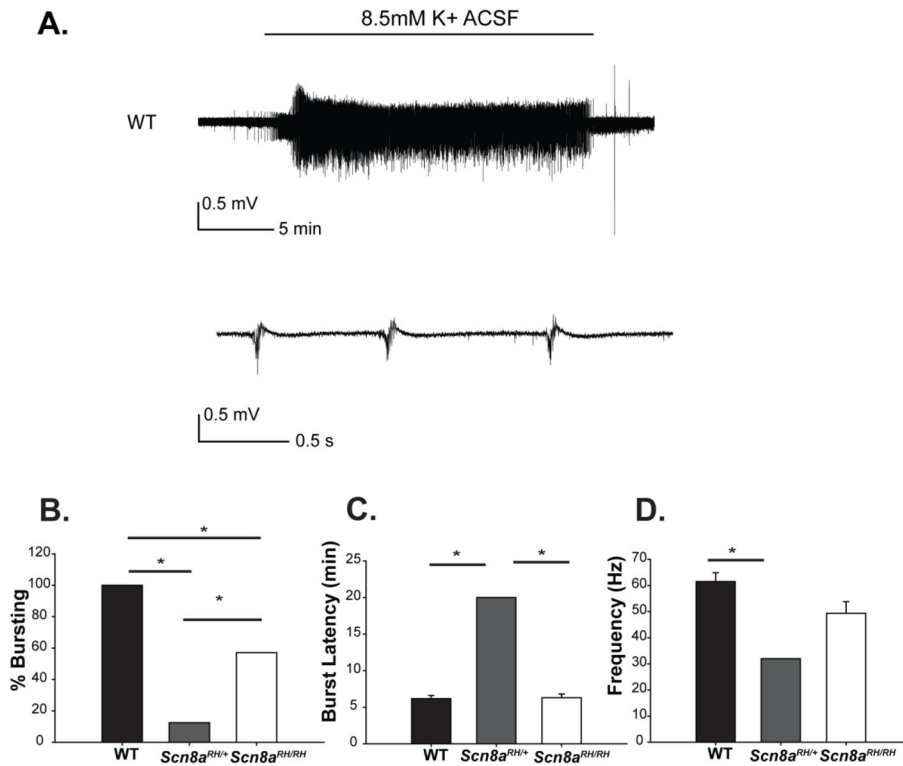
Characterization of the biophysical properties of R1627H channels in *Xenopus* oocytes. A and B. Sample two-electrode voltage clamp recordings of currents through wild-type $\text{Na}_v1.6$ (A) and R1627H channels (B) with co-expression of $\beta 1$ during depolarizations between -50 and $+50$ mV in 10 mV increments. C. The R1627H mutation leads to a depolarizing shift in the $V_{1/2}$ of voltage-dependent activation (Student's *t* test, $P < 0.05$). D. R1627H channels have accelerated recovery from inactivation (two-way ANOVA, Holm-Sidak correction, $P < 0.05$). E. At holding potentials from -30 to $+40$ mV, R1627H channels exhibit increased persistent current (two-way ANOVA, Holm-Sidak correction, $P < 0.05$). F. The R1627H mutation decreased use-dependent inactivation at 30 Hz (two-way ANOVA, Holm-Sidak correction, $P < 0.05$).

**FIGURE 2.**

Recessive motor impairment in R1627H mice. **A.** Locomotor activity of *Scn8a*-R1627H mice in a new cage was measured over a 24-hour period. A significant deficit in locomotor activity was detected between *Scn8a*^{RH/RH} mice and WT littermates (two-way ANOVA, genotype X time, $P < 0.05$). No significant differences were detected between *Scn8a*^{RH/+} and WT littermates ($P > 0.05$). Inset graph shows reduced locomotor activity of *Scn8a*^{RH/RH} mice during the initial period in a novel environment ($P < 0.05$). White and black bars under the X-axis represent the light-dark cycle. $n = 9-12$. **B.** Rotarod performance was reduced in *Scn8a*^{RH/RH} (red) but not WT (black) or *Scn8a*^{RH/+} (blue) mice (one-way ANOVA, $P < 0.001$, Dunnett's *post hoc*, $P < 0.05$, $n = 7-18$). **C.** Representative example of paw prints showing reduced stride length in *Scn8a*^{RH/RH} mice. Black lines show relative stride length. **D.** Stride lengths were found to be significantly reduced in *Scn8a*^{RH/RH} but not *Scn8a*^{RH/+} mice when compared to WT littermates (one-way ANOVA, $P < 0.001$; Dunnett's *post hoc*, $P < 0.05$). Error bars represent SEM, $n = 6-10$.

**FIGURE 3.**

Effects of the R1627H mutation on fluoroethyl- and 6 Hz-induced seizure susceptibility. A. *Scn8a^{RH/+}* but not *Scn8a^{RH/RH}* mice have longer latencies to fluoroethyl-induced seizures when compared to WT littermates (one-way ANOVA, MJ and GTCS, Tukey *post hoc*, * $P < 0.05$, $n = 11-12$). B. Seizure severity, as measured by hindlimb extension (HE) and death, were reduced in *Scn8a^{RH/+}* and *Scn8a^{RH/RH}* mice (χ^2 , * $P < 0.05$). C. *Scn8a^{RH/+}* mice are more resistant to 6 Hz seizures compared to *Scn8a^{RH/RH}* and WT littermates. D. Both *Scn8a^{RH/+}* and *Scn8a^{RH/RH}* mice experience less severe seizures in response to stimulus intensities of 20, 22, and 24 mA compared to WT littermates (one-way ANOVA, $P < 0.0001$, Dunnett's *post hoc*, $P < 0.001$, $n = 8-10$).

**FIGURE 4.**

Effects of the R1627H mutation on hippocampal bursting. A. Example of bursting observed during field recording from WT CA3 when bath solution is switched from regular ACSF to high K⁺ ACSF. Bursting stops soon after high K⁺ ACSF is replaced with regular ACSF. B. The percentage of slices that exhibited bursting in the presence of high K⁺ was WT (5/5, 100%), *Scn8a*^{RH/+} (1/8, 12.5%), and *Scn8a*^{RH/RH} (4/7, 57.1%, *P < 0.05, Fisher Exact Test). C. The latency to the occurrence of bursting activity in the presence of high potassium (K⁺) was increased in slices from *Scn8a*^{RH/+} but not WT or *Scn8a*^{RH/RH} littermates. D. The frequency of intra-burst high amplitude spiking activity was reduced in *Scn8a*^{RH/+} compared to WT and *Scn8a*^{RH/RH} littermates. (B and C, data are average ± SEM, *P < 0.05, one-way ANOVA, Holm-Sidak *post-hoc* test).

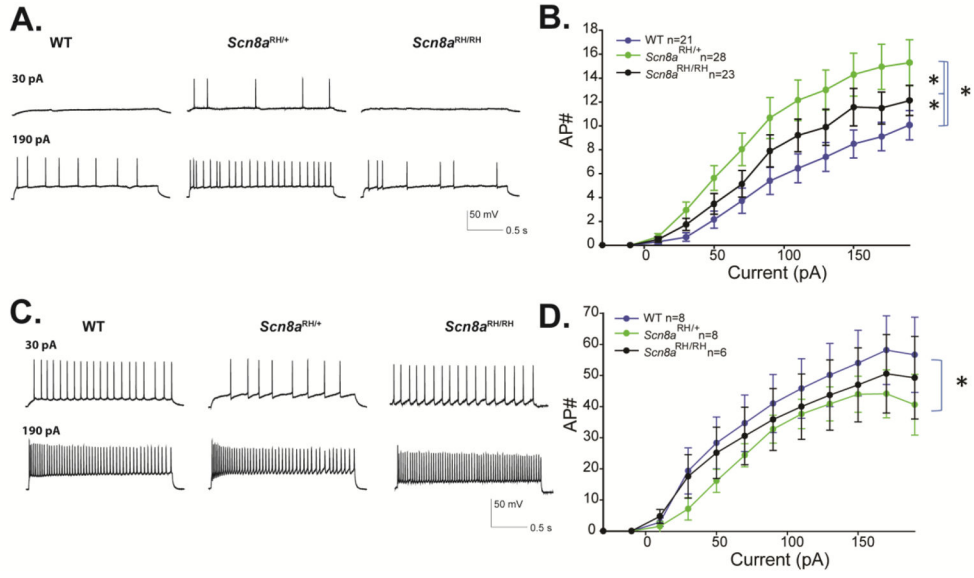
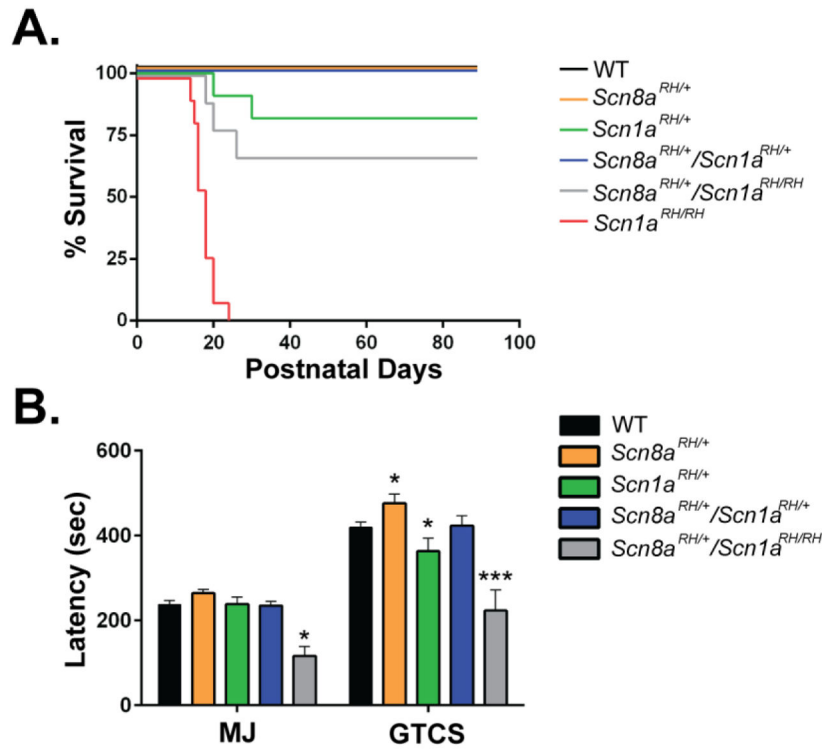
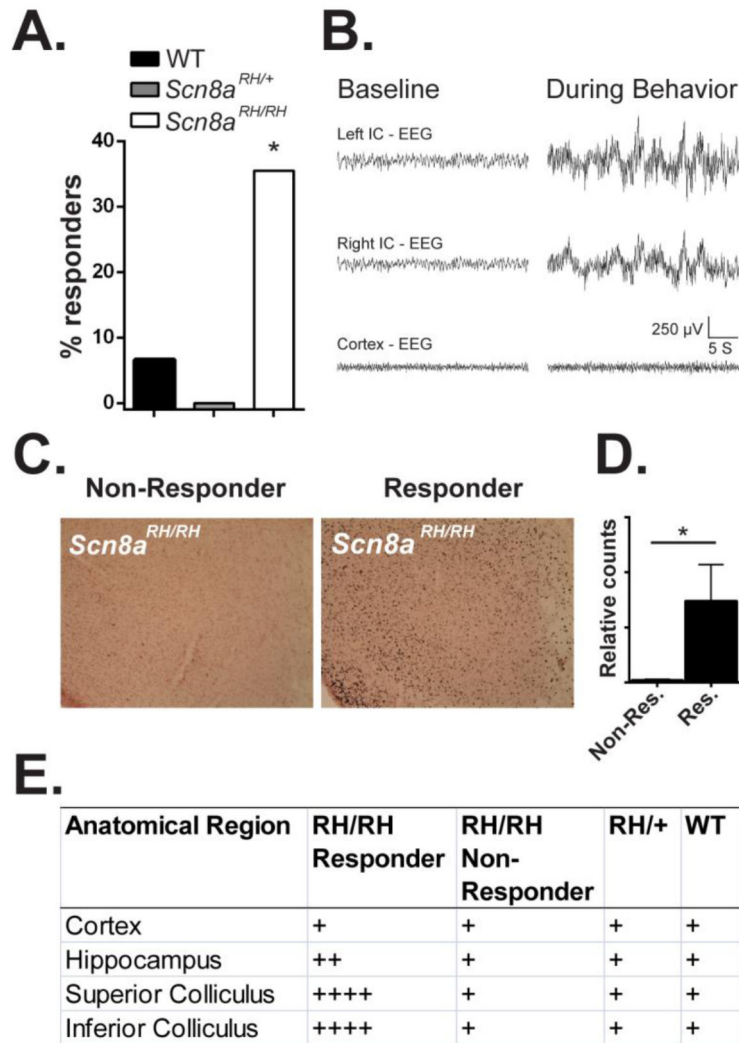


FIGURE 5. Firing properties of CA3 neurons from R1627H mice. A. Sample traces from CA3 pyramidal neurons of WT, *Scn8a*^{RH/+} and *Scn8a*^{RH/RH} mice at depolarizing current injections of 30 and 190 pA from a resting potential of -70mV. B. Average number of action potentials (AP#) plotted against current injection (pA) (Error bars represent SEM, n = number of cells ; *P < 0.05, two-way ANOVA, Holm-Sidak correction). C. Sample traces from CA3 interneurons of WT, *Scn8a*^{RH/+} and *Scn8a*^{RH/RH} mice at depolarizing current injections of 30 and 190 pA from a resting potential of -70 mV. B. Average number of action potentials (AP#) plotted against current injection (pA). Error bars represent SEM, n = number of cells, *P < 0.05 two-way ANOVA, Holm-Sidak correction.

**FIGURE 6.**

The *Scn8a*-R1627H mutation increases lifespan and seizure resistance in a mouse model of GEFS+ (*Scn1a*-R1648H). A. No mortality was observed over the first three months of postnatal development in WT, *Scn8a*^{RH/+}, and *Scn1a*^{RH/+}/*Scn8a*^{RH/+} mice. In contrast, *Scn1a*^{RH/+} and *Scn1a*^{RH/RH} mice experienced 18% (2/11) and 100% (11/11) mortality, respectively. *Scn1a*^{RH/RH}/*Scn8a*^{RH/+} mice exhibited 40% (4/10) survival. B. *Scn1a*^{RH/+} mutants (green) have lower latencies to flurothyl-induced GTCS, while *Scn8a*^{RH/+} mutants (orange) exhibit elevated latencies when compared to WT littermates. Normal latencies were restored in *Scn1a*^{RH/+}/*Scn8a*^{RH/+} mice (blue). *Scn1a*^{RH/RH}/*Scn8a*^{RH/+} mice (grey) have reduced latencies to the MJ and GTCS. One-way ANOVA, Dunnett's *post hoc*, *P < 0.05, ***P < 0.001. Error bars represent SEM, n = 5–17.

**FIGURE 7.**

Brainstem activity in *Scn8a*^{RH/RH} mice following sound-induced wild-running behavior. A. *Scn8a*^{RH/RH}, *Scn8a*^{RH/+}, and WT mice were exposed to 5-minute duration tones (12 kHz, 80 dB) or broad-spectrum (13–85 kHz, 50–80 dB) acoustic stimuli. Approximately 7% (1/15) of WT, 0% (0/10) of *Scn8a*^{RH/+}, and 36% (11/31) of *Scn8a*^{RH/RH} mice exhibited wild running behavior during sound stimulus presentation (χ^2 , *P < 0.05). B. Representative example of inferior colliculus (IC) and cortical EEG activity in an *Scn8a*^{RH/RH} mouse before (baseline) and during abnormal behavior. C. Representative image of c-Fos expression in the IC of a responding and non-responding *Scn8a*^{RH/RH} mouse 2 hours after exposure to sound stimulus. D. Increased c-Fos immunoreactive cells were observed in the IC of responding compared to non-responding *Scn8a*^{RH/RH} mice 2 hours following exposure to acoustic stimuli (Mann-Whitney U test, *P < 0.05, Error bars represent SEM, n = 3–4). E. Regional expression of c-Fos 2 hours after exposure to sound stimulus. Relative c-Fos expression: (+) low; (++) light; (+++) moderate; (++++) high. High levels of c-fos expression were observed in the superior and inferior colliculus of *Scn8a*^{RH/RH} responding animals but not in

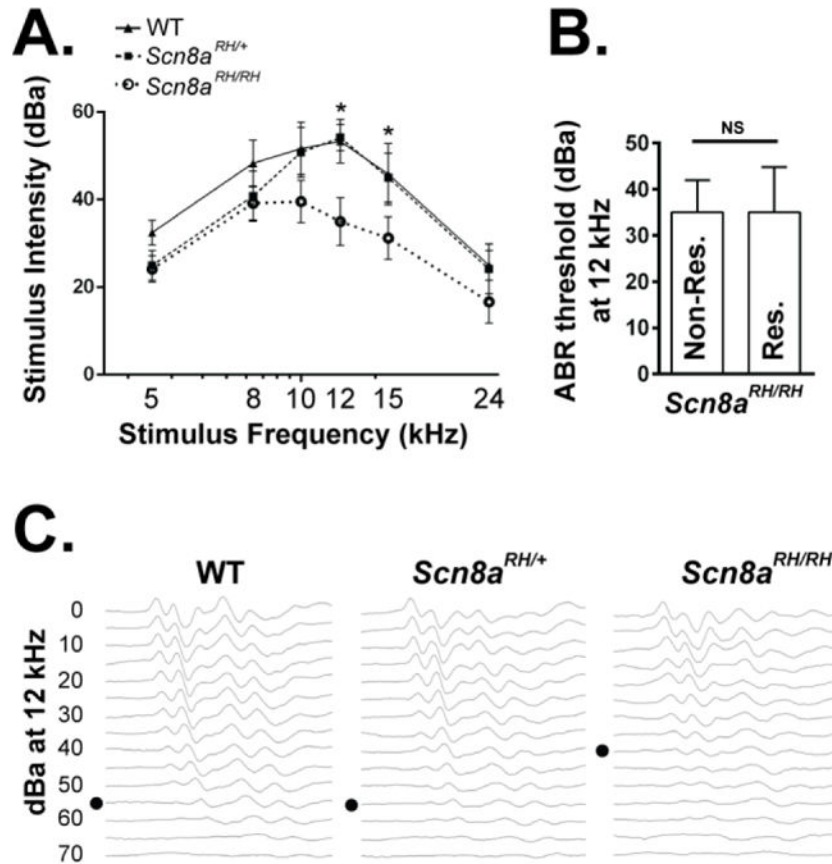
non-responding *Scn8a^{RH/RH}*, *Scn8a^{RH/+}* or WT littermates. Low to light levels of c-Fos was observed in the hippocampus and cortex of all animals.

Author Manuscript

Author Manuscript

Author Manuscript

Author Manuscript

**FIGURE 8.**

Scn8a^{RH/RH} mice have reduced auditory brainstem nuclei responses (ABRs). A. Auditory brainstem nuclei responses (ABR) were measured in response to 5–24 kHz tones in WT, *Scn8a*^{RH/+} and *Scn8a*^{RH/RH} mice. *Scn8a*^{RH/RH} mice were found to have reduced auditory responses between 12–15 kHz (two-way ANOVA, Dunnett's *post hoc*, * $P < 0.05$, $n = 8-10$). B. No differences in ABR thresholds at 12 kHz were observed between *Scn8a*^{RH/RH} mice that did not display wild-running behavior (non-responders) and *Scn8a*^{RH/RH} mice that did exhibit abnormal behavior (responders) (Student's *t* test, $P > 0.05$, $n = 4-8$). C. Representative examples of ABR responses in WT and R1627H mutant mice. Black dot indicates the response threshold. Error bars represent SEM.

TABLE 1

Summary of survival and behavioral assessment of the R1627H line.

Category	Test	# of Animals	Measurement	Genotype	Average	s.e.m.	p	Post hoc Test	Comparison	Significance									
Survival	Survival	WT = 24 RH/+ = 36 RH/RH = 28	4 mo % mortality	WT	0.0	-	-			-									
				RH/+	0.0	-													
				RH/RH	0.0	-													
Anxiety	Elevated Plus Maze	WT = 10 RH/+ = 12 RH/RH = 10	% time in open arm	WT	25.1	3.8	0.84				-								
				RH/+	26.9	2.6													
				RH/RH	28.6	5.5													
				Anxiety	Elevated Plus Maze	WT = 10 RH/+ = 12 RH/RH = 10	Open arm entries	WT	13.3	2.5	0.73				-				
								RH/+	12.1	1.6									
								RH/RH	10.8	2.4									
								Anxiety	Elevated Plus Maze	WT = 10 RH/+ = 12 RH/RH = 10	Distance traveled (cm)	WT	106.2	8.1	0.64				-
												RH/+	115.9	7.3					
												RH/RH	104.6	12.6					
Anxiety	Open Field	WT = 8 RH/+ = 12 RH/RH = 10	Time in center (sec)									WT	5.3	5.5	0.05				-
												RH/+	7.9	8.5					
												RH/RH	1.1	2.0					
				Anxiety	Open Field	WT = 8 RH/+ = 12 RH/RH = 10	Number of entries into the center					WT	2.8	2.1	$p < 0.01$	Dunnett's Test		WT vs. RH/+	$p > 0.05$
												RH/+	3.6	2.5					
												RH/RH	0.6	0.7					
								Anxiety	Open Field	WT = 8 RH/+ = 12 RH/RH = 10	Latency to first center entry (sec)	WT	67.3	86.4	0.23				-
												RH/+	132.0	93.9					
												RH/RH	65.6	108.6					
Depression-like	Forced Swim	WT = 10 RH/+ = 10 RH/RH = 10	Time swimming (sec)									WT	90.1	10.3	0.57				-
												RH/+	83.6	11.2					
												RH/RH	99.5	8.6					
				Depression-like	Forced Swim	WT = 10 RH/+ = 10 RH/RH = 10	Time floating (sec)					WT	122.2	22.3	0.2				-
												RH/+	121.5	24.5					
												RH/RH	71.2	15.8					

Category	Test	# of Animals	Measurement	Genotype	Average	s.e.m.	p	Post hoc Test	Comparison	Significance
Learning/Memory	Tail Suspension	WT = 10 RH/+ = 15 RH/RH = 10	Time struggling (sec)	WT	170.7	8.4	$p < 0.01$	Dunnett's Test	-	-
				RH/+	171.8	10.6			WT vs. RH/+	$p > 0.05$
				RH/RH	247.7	7.2			WT vs. RH/RH	$p < 0.05$
				WT	229.5	5.0			-	-
				RH/+	220.7	12.9			WT vs. RH/+	$p > 0.05$
				RH/RH	164.1	8.5			WT vs. RH/RH	$p < 0.05$
	Sucrose Preference	WT = 11 RH/+ = 10 RH/RH = 11	Sucrose preference (sucrose g/ total g) *100	WT	96.9	2.9	0.64	-	-	-
				RH/+	97.0	1.9			-	-
				RH/RH	89.5	10.7			-	-
				WT	59.7	4.9			-	-
				RH/+	62.1	6.8			0.77	-
				RH/RH	55.1	10.9			-	-
Novel Object Recognition (20 min exposure)	WT = 8 RH/+ = 10 RH/RH = 12	Novel object preference	WT	56.2	4.9	0.41	-	-	-	
			RH/+	62.6	6.8			-	-	
			RH/RH	64.8	10.9			-	-	
			WT	69.6	10.3			-	-	
			RH/+	58.5	8.8			0.923	-	
			RH/RH	66.4	7.8			-	-	
Novel Object Recognition (5 min exposure)	WT = 8 RH/+ = 10 RH/RH = 12	Novel position preference	WT	61.9	10.8	0.136	-	-	-	
			RH/+	60.6	5.9			-	-	
			RH/RH	70.9	13.0			-	-	
			WT	59.3	2.2			-	-	
			RH/+	56.8	1.4			0.031	Dunnett's Test	
			RH/RH	64.2	6.4			-	-	
Y-Maze	WT = 10 RH/+ = 12 RH/RH = 10	% correct rotations	WT	331.4	19.3	0.021	Dunnett's Test	-	-	
			RH/+	352.3	18.7			WT vs. RH/+	$p > 0.05$	
			RH/RH	264.3	27.11			WT vs. RH/RH	$p > 0.05$	
			WT	59.3	2.2			-	-	
			RH/+	56.8	1.4			0.031	Dunnett's Test	
			RH/RH	64.2	6.4			-	-	

Mice carrying the R1627H mutation and WT littermates were evaluated for survival and were subjected to a battery of behavioral tests in order to evaluate anxiety, depressive-like, and learning and memory related behaviors.

TABLE 2

Intrinsic properties of hippocampal neurons from R1627H mice.

	AP properties of pyramidal cells				AP properties of interneurons			
	Amplitude (mV)	Threshold (mV)	Half-width (ms)	N	Amplitude (mV)	Threshold (mV)	Half-width (ms)	N
WT	87 ± 2	-45 ± 1	2 ± 0.1	21	80 ± 5	-49 ± 2	2 ± 0.2	8
RH/+	88 ± 2	-46 ± 1	2.3 ± 0.1*	28	81 ± 4	-43 ± 2	2.5 ± 0.1	8
RH/RH	78 ± 3*	-46 ± 2	2.7 ± 0.1*	23	80 ± 4	-45 ± 3	2.6 ± 0.4	6

Summary of intrinsic membrane properties of hippocampal pyramidal cells and interneurons obtained by current clamp recording (one-way ANOVA, Holm-Sidak test).

Values represent average ± SEM, n = number of cells,

* P < 0.05.